Global Change Biology (2003) **9,** 547–562

Carbon emissions from fires in tropical and subtropical ecosystems

GUIDO R. VAN DER WERF*, JAMES T. RANDERSON†, G. JAMES COLLATZ‡ and LOUIS GIGLIO§

**USDA-FAS, NASA Goddard Space Flight Center, Code 923, Greenbelt Road, Greenbelt, MD 20771, USA, †Divisions of Geological and Planetary Sciences and Engineering and Applied Science, California Institute of Technology, Mail stop 100-23, Pasadena, CA 91125, USA, ‡NASA Goddard Space Flight Center, Code 923, Greenbelt Road, Greenbelt, MD 20771, USA, §Science Systems and Applications Inc., NASA Goddard Space Flight Center, Code 923, Greenbelt Road, Greenbelt, MD 20771 USA*

Abstract

Global carbon emissions from fires are difficult to quantify and have the potential to influence interannual variability and long-term trends in atmospheric CO_2 concentrations. We used 4 years of Tropical Rainfall Measuring Mission (TRMM) Visible and Infrared Scanner (VIRS) satellite data and a biogeochemical model to assess spatial and temporal variability of carbon emissions from tropical fires. The TRMM satellite data extended between 38°N and 38°S and covered the period from 1998 to 2001. A relationship between TRMM fire counts and burned area was derived using estimates of burned area from other satellite fire products in Africa and Australia and reported burned areas from the United States. We modified the Carnegie-Ames-Stanford-Approach (CASA) biogeochemical model to account for both direct combustion losses and the decomposition from fire-induced mortality, using both TRMM and Sea-viewing Wide Field of view Sensor (SeaWiFS) satellite data as model drivers. Over the 1998–2001 period, we estimated that the sum of carbon emissions from tropical fires and fuel wood use was 2.6 Pg C yr^{-1}. An additional flux of 1.2 Pg C yr^{-1} was released indirectly, as a result of decomposition of vegetation killed by fire but not combusted. The sum of direct and indirect carbon losses from fires represented 9% of tropical and subtropical net primary production (NPP). We found that including fire processes in the tropics substantially alters the seasonal cycle of net biome production by shifting carbon losses to months with low soil moisture and low rates of soil microbial respiration. Consequently, accounting for fires increases growing season net flux by ~12% between 38°N and 38°S, with the greatest effect occurring in highly productive savanna regions.

Keywords: biomass burning, fire ecology, global carbon cycle, net primary production, TRMM

Received 9 August 2002; revised version received and accepted 10 July 2002

Introduction

Biomass burning and wildfires play an important role in the cycling of carbon in many ecosystems and represent a significant source of aerosols and trace gas emissions, particularly in tropical and boreal regions (Crutzen & Andreae, 1990; Hao *et al*., 1990; Kasischke *et al*., 1995). Within the tropics, fire return times (FRTs) vary widely, and depend on climate, vegetation type, and human activity (Menaut *et al*., 1991). Some savannas burn every year, while moist tropical forests rarely burn. The large fires in Brazil and Indonesia during the 1997–1998 El Niño-Southern Oscillation (ENSO) event demonstrate, however, that under extreme climatic conditions even closed canopy rainforests can burn extensively, especially when promoted by humans (Cochrane *et al*., 1999; Nepstad *et al*., 1999; Siegert *et al*., 2001).

Approaches used for estimating emissions from fires have evolved over the last two decades to take advantage of new satellite data products, improved GIS capabilities, and more comprehensive biogeochemical models. Early studies estimated carbon losses from fires on a continental or global scale by developing inventories of aggregated

Correspondence: G. R. van der Werf, USDA-FAS, NASA Goddard Space Flight Center, Code 923, Greenbelt Road, Greenbelt, MD 20771, USA, fax +1 301 614 6695,
e-mail: guido@ltpmail.gsfc.nasa.gov

fuel, combustion factors, and fire return times for different biome types, and then extrapolating regional emissions estimates using global vegetation maps. Initial estimates of emissions from this inventory approach varied between 1.5 and 5.0 $Pg\,C\,yr^{-1}$ (Seiler & Crutzen, 1980; Crutzen & Andreae, 1990; Hao *et al.*, 1990; Hao & Liu, 1994).

The use of satellite observations has generally led to a decrease in emission estimates, and to greater recognition of the importance of spatial and temporal variability in fire frequency. The two primary ways of assessing burned area with remote sensing are (1) indirectly by detecting active fires (hot spots or smoke) and converting these to burned areas, and (2) directly by measuring fire scars, based on changes in surface reflectance (or vegetation indices) before and after fire (Eva & Lambin, 1998). Sometimes the two approaches are combined, with hot spot algorithms applied over large regions, and validated with burned scar information from high-resolution satellite imagery from a few specific locations. For example, Setzer & Pereira (1991) assessed burned area in the Amazon using Advanced Very High Resolution Radiometer (AVHRR) fire counts scaled to burned area derived from Landsat/TM data. Using an indirect satellite method, Scholes *et al*. (1996) showed that the inventory-based methods overestimated burned areas when FRTs from productive savanna and other ecosystems that burn frequently were assumed to represent larger regions. In the Scholes *et al*. (1996) analysis, satellite measurements showed that fire frequency was reduced in many areas that had bare patches, cities, and lower productivity ecosystems. Using a direct satellite-based measurement of fire scars, Barbosa *et al*. (1999a) obtained burned areas for southern Africa that had considerable interannual variability, but with a mean comparable to the earlier estimates from Scholes *et al*. (1996). During the 1980s in Africa, they found that emissions in a high fire year were double those in a low fire year.

While satellite data has vastly improved our capability to assess heterogeneity in burned areas in non-forested ecosystems, many remote sensing approaches have had limited success in detecting fire in or under closed canopy forests. Pereira *et al*. (1999) addressed the need for accurately assessing burned areas in tropical forest and other forested areas; although the area burned annually in tropical forest is much smaller than in savannas, the amount of fuel is large so emissions from forested areas can be significant. For example, Potter *et al*. (2001) used fire counts scaled to satellite-derived deforestation rates (indirect method) to obtain an emissions estimate of 0.71 $Pg\,C\,yr^{-1}$ for the Legal Amazon, nine times higher than the estimate for southern Africa by Scholes *et al*. (1996). In comparing southern Africa and Amazon emissions, it is important to note that less than 15% of the fires detected in the Amazon occurred in the tropical forests and that the fuel loads and combustion factors varied considerably between the two studies.

While burned area estimates have improved with the use of satellite data, large uncertainties remain. The fire count approach using hot spot detection may miss fires that occur mostly outside of the overpass time and ground fires under closed canopy forests and woodlands. Smoke and clouds may also interfere with the detection of hot spots. More fundamentally, the nature of the relationship between the number of fires and their sizes may be variable and other types of information may be necessary to specify that relationship with useful accuracy. Direct measurement of burn scars from satellites can also miss small fires and understorey fires and may have difficulty in attributing changes in surface reflectance to burned area.

Some of the uncertainty in estimating large-scale emissions using inventory methods or satellite based methods comes from the difficulty of scaling local measurements to larger regions such as grid cells in global models. Many field campaigns focusing partly or completely on biomass burning in the tropics [including the Southern Africa Fire-Atmosphere Research Initiative (SAFARI, Lindesay *et al*., 1992), and Experiment for Regional Sources and Sinks of Oxidants (EXPRESSO, Delmas *et al*., 1999)] have provided key information on combustion factors and fuel loads. However, applying this information to regional or continental scales remains difficult because of limited information on the distribution of fuels, and on the fire-induced mortality of woody vegetation in tropical regions.

Here we explore the effects of fire on carbon cycling in the global tropics and subtropics (between 38°N and 38°S) along a precipitation-driven vegetation gradient. In our analysis, we partition the tropics into 6 classes based on precipitation and tree cover. Within each vegetation class, we then estimate the effects of fire on ecosystem processes, including FRT, emissions, indirect losses (from fire-induced mortality), herbivory (competing with fire as a loss pathway), and fuel wood consumption. We use satellite datasets from the Tropical Rainfall Measuring Mission (TRMM) and Sea-viewing Wide Field of view Sensor (SeaWiFS) as inputs to a global biogeochemical model (CASA, Carnegie-Ames-Stanford Approach) that accounts for the effects of fire on carbon stocks, on fluxes from fires and respiration and on net biome productivity. Other processes considered include fuel wood consumption and herbivory. The advantage of embedding fire emission processes within a biogeochemical model is that we can compare fire with other ecosystem processes in terms of their impact on carbon fluxes. The disadvantage is that our global modelling framework may misrepresent key regional scale processes that affect emissions, including the relationship between burned area and satellite fire index.

We obtain fire location and timing from the analysis of hot spots detected by the Visible and Infrared Scanner (VIRS) instrument on board the TRMM satellite platform (Giglio *et al*., 2002) and compare these data with other published estimates. We show that fires consume ~6% of annual NPP within 38°N and 38°S, substantially alter the seasonal cycle of net biome production, and have the greatest impact on carbon fluxes in biomes with intermediate levels of moisture.

Methods

We calculated the amount of carbon combusted during fires, C at each grid cell, and month (t) using the following relationship (modified from Seiler & Crutzen, 1980):

$$C_t = A_t f_c \left[\sum^{d} E_d \, D_{t,d} + \sum^{b} E_b \, M_b \, B_{t,b} \right] + f_c \, E_F \, F \qquad (1)$$

where A is the area burned, D is the dead plant material (detritus), B is the living plant material (biomass), f_c is the fraction of carbon in the fuel (0.45), M is the mortality factor (which only operates on biomass), and E the combustion factor (the fraction of the fuel that was combusted). E, M, D and B vary among the different detritus (d) and biomass (b) pools (i.e. surface litter, coarse woody debris, living leaf, and living stem pools). The last term in Eqn (1) accounts for the amount (F) and combustion efficiency (E_F, set to 1.0) of fuel wood. We obtained A_t by deriving a relationship between TRMM satellite fire counts and burned area using regionally based estimates (described below). The formation of black carbon was not explicitly treated in our model because it is relatively inert on the seasonal and interannual timescales that were the focus of this study. We solved Eqn (1) using the CASA biogeochemical model modified for fires and fuel wood consumption. E was estimated from plant tissue dependent combustion factors, and the fraction of wood, leaves, and detritus in a grid cell. F was estimated from maps of population density and per capita estimates of consumption (described below). With CASA, we were able to use other ecological and satellite data to constrain NPP, allocation of NPP, and decomposition. CASA allowed us also to track the decomposition of biomass from fire-induced mortality (hereafter referred to as an indirect loss).

TRMM fire counts and burned area

The TRMM satellite was launched in November 1997 and is currently projected to collect data for about 8 years. The orbit of the TRMM satellite is inclined at 35° so that the sensors on board of the satellite observe the earth between 38°N and 38°S (Kummerow *et al*., 1998). The frequency of overpasses at any location within this region depends on the latitude; at equatorial latitudes two observations are made every other day, at higher latitudes two to three observations are made daily (Giglio *et al*., 2002). Local overpass time progresses over the 24-h diurnal cycle roughly once per month. The TRMM satellite carries the Visible and Infrared Scanner (VIRS), an imaging radiometer with five channels between 0.6 and 12 μm, and a nadir spatial resolution of 2.1 km. An existing AVHRR algorithm was modified to detect fires with VIRS, based on the brightness temperature of channel 3 (3.75 μm) and channel 4 (10.8 μm) and the surface reflectance of channel 2 (1.6 μm); the detected fire pixels are then used to produce a monthly, coarse-resolution ($0.5^\circ \times 0.5^\circ$) fire product that includes corrections for missing data and the variable number of observations made at different latitudes (Giglio *et al*., 2002, available online at http://daac.gsfc.nasa.gov/CAMPAIGN_DOCS/hydrology/TRMM_VIRS_Fire.shtml). One advantage of TRMM's orbital characteristics over platforms in sun-synchronous orbits is that, because the TRMM overpass time varies on a daily basis, diurnal patterns of burning may be observed (Giglio *et al*., 2000). Sun-synchronous platforms on the other hand, which include most polar orbiters, restrict observations to the same local times each day.

To obtain a relationship between fire counts and burned area, we used burned area estimates derived from the MODIS (MODerate resolution Imaging Spectrometer) instrument, on board the NASA Terra satellite, using a newly developed algorithm which is based on detecting changes in vegetation indexes at 500-meter resolution. We also used burned area estimates provided by the National Interagency Coordination Center (NICC), which gives monthly burned areas for regions within the US (available online: http://www.cidi.org/wildfire/index.html). The TRMM fire counts capture seasonal variability of burned area within the state of California (Fig. 1).

We made the relationship between burned area and fire counts a linear function of tree cover in regions with less than 40% tree cover based on a comparison of TRMM fire counts with MODIS burned area (Fig. 2). In this analysis we used four MODIS tiles, each $\sim 10^\circ \times 10^\circ$ from Australia (2), West Africa (1), and southern Africa (1). Within each tile, the 500-meter resolution MODIS burned area was aggregated to $0.5^\circ \times 0.5^\circ$ resolution and compared with the TRMM fire count product, which is also aggregated to $0.5^\circ \times 0.5^\circ$ resolution. The ratio between burned area and fire counts was then related to the percentage tree cover (DeFries *et al*., 1999), which was the average value for the corresponding $0.5^\circ \times 0.5^\circ$ grid cell. As shown in Fig. 2 the burned area per fire count decreases with increasing percentage tree cover. One possible reason for this trend is the difference in fire spreading rate: a fire in a grassland spreads quickly

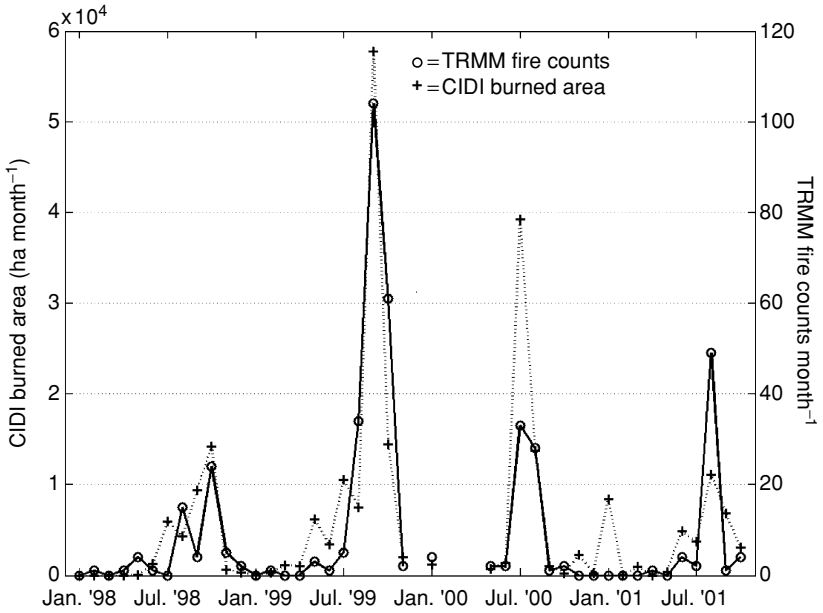

Fig. 1 Burned area as reported by NICC compared with TRMM fire counts for the southern part of California.

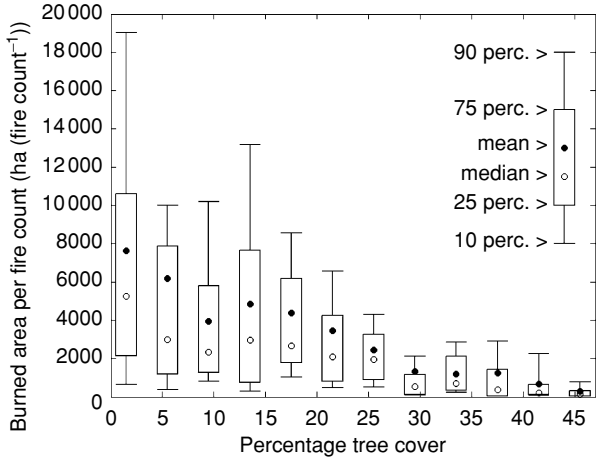

Fig. 2 The relationship between burned area and TRMM fire counts depends on tree cover. Burned area is derived from a change in MODIS vegetation index. Both TRMM fire counts and MODIS burned area were aggregated to $0.5^\circ \times 0.5^\circ$ for this comparison. Percentage tree cover (average value for the corresponding $0.5^\circ \times 0.5^\circ$ grid cells) from DeFries *et al.* (1999). Perc. is percentile.

and burns for a short period. This results in a lower detection probability of hot spots and thus a higher burned area per detected fire count. Another explanation may be that the drop in vegetation index in a grassland may be bigger than the drop in a more wooded area; the trees, which may cause most of the vegetation index signal may be unaffected by the fire.

To serve as input data in our model, the $0.5^\circ \times 0.5^\circ$ TRMM fire counts were binned to $1^\circ \times 1^\circ$ and the burned area was then calculated using the tree cover dependant fire count to burned area ratio as presented in Fig. 3. Further testing, refinement and validation of the algorithm for transforming TRMM fire counts into burned area is underway (Giglio *et al.* in preparation) and will likely lead to improved accuracy in fire emission estimates. One factor likely to be important in estimating emissions that is not explicitly addressed in this paper is the actual area burned within the boundaries of an identified fire scar. Within a fire perimeter, patches of land may undergo varying degrees of combustion completeness as a result of variability in moisture, fuel load, and topography. For the burned area calculation we assumed that a MODIS 500 meter grid cell was either completely burned or was completely unburned. In some areas, this may have led to an overestimation of actual area burned. This bias may have been compensated for in other areas where the fire scar was not large enough to be detected.

We investigated the sensitivity of predicted burned area and emissions to our assumptions about the relationship between burned area per fire count and percentage tree cover with two additional scenarios (Fig. 3). The sensitivity of our results to a possible underestimation of burned area in closed woody canopies was assessed by prescribing burned area per fire pixel as independent of amount of tree cover when this value exceeded 35% (scenario 1 in Fig. 3). In a second test (scenario 2), we scaled our original function so that the total area burned for Africa matched the total area burned from the mean of the upper and lower scenarios given by Barbosa *et al.* (1999b) and we applied this relationship to the entire model domain. In these alternative scenarios we

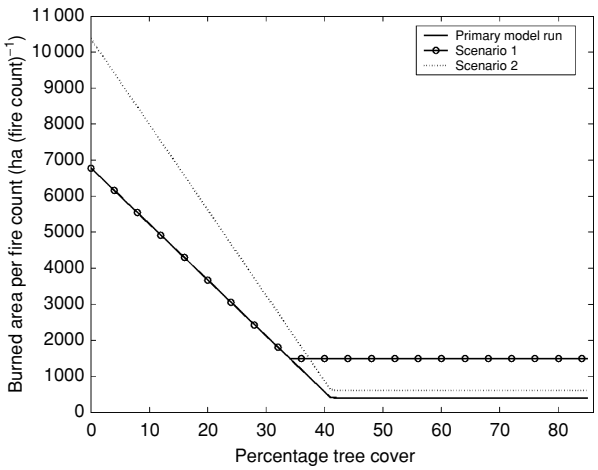

Fig. 3 Different scenarios for scaling burned area to fire counts. The primary model run is used throughout this study, scenario 1 is the same as the primary model run except the relation is set to be independent of percentage tree cover at a lower tree cover percentage, scenario 2 represents the scaling of the primary model run to match burned areas reported by two other studies.

maintained the decreasing area burned per fire count with increasing tree cover relationship derived from our analysis of the MODIS burned areas.

The CASA biogeochemical model

The Carnegie-Ames-Stanford Approach (CASA) biogeochemical model was designed for simulating net carbon fluxes from the terrestrial biosphere on timescales from seasons to centuries (Potter *et al*., 1993). For this study the model operates at a $1^\circ \times 1^\circ$ spatial resolution and with a monthly time step. Satellite-derived estimates of fraction of incident photosynthetically active radiation (PAR) absorbed by the green plant canopy (FPAR) were obtained from SeaWiFS (Behrenfeld *et al*., 2001), averaged over the September 1997–August 2000 period. Estimates of PAR were derived from satellite-based estimates of solar insolation based on monthly averages for the period 1983–1991 (Bishop & Rossow, 1991). Net primary production (NPP) was calculated for each month and $1^\circ \times 1^\circ$ grid cell from the absorbed PAR (FPAR $\times$ PAR) and a light use efficiency ε that depended locally on temperature (T) and soil moisture stress (P) (Field *et al*., 1995, 1998):

$$\mathrm{NPP} = \varepsilon_{(T,P)} \times \mathrm{FPAR} \times \mathrm{PAR} \qquad (2)$$

We set the maximum light use efficiency in our model runs at $0.5\,\mathrm{g\,C\,MJ^{-1}}$ PAR based on previous atmospheric inversion analyses that used the seasonal cycle of atmospheric CO_2 as a constraint (Randerson *et al*., 2002). NPP and decomposition are scaled by soil moisture and temperature (derived from global monthly maps of temperature and precipitation, Leemans & Kramer, 1990; W. Cramer, unpublished data, 1994). NPP was allocated to leaves, wood, and fine roots with a ratio of 1:1:1 for woody vegetation, and a ratio of 1:1 for leaves and fine roots in herbaceous vegetation. Fractional woody and herbaceous vegetation was separately estimated for each grid cell as described by Defries *et al*. (2000). This approach allowed us to capture spatial variability in woody biomass and fuels in regions that fall in between closed tropical forests and grasslands that would be missed by a discrete vegetation classification.

The seasonality in the delivery of leaves and fine roots to the litter pools was estimated from changes in satellite-derived leaf area (Randerson *et al*., 1996). Decomposition of plant litter and soil organic matter transformations depended on soil moisture, temperature, and the chemical composition (C:N ratio and lignin) of plant litter (Parton *et al*., 1993).

Modifications of CASA to account for fire

Fires represent a potentially significant loss pathway for aboveground biomass and litter. The fraction of aboveground biomass and litter affected by fire was calculated from the ratio of burned to total area within each grid cell. Burning initiated a direct loss of carbon from aboveground carbon pools, depending on mortality and combustion factors described below (Fig. 4).

We scaled the mortality of woody vegetation with the amount of tree cover so that a grid cell with a high percentage tree cover had a high mortality, while the mortality of woody vegetation in an open grassland was low (the algorithm is defined in Table 1): the grasslands that surround individual mature trees normally lack sufficient fuel to produce high flames that can kill the trees (Medina & Silva, 1990). Furthermore, many woody species in biomes with high fire frequencies have an insulating bark that protects them against fires (Gill, 1981). For the herbaceous component of the vegetation we assumed that all aboveground living biomass died in a fire while 90% of the roots survived (Table 1). The combustion factors we used vary between different fuel types (Table 1) and are averages from detailed studies by Shea *et al*. (1996) and Hoffa *et al*. (1999).

The aboveground living biomass that was killed but not combusted entered the aboveground litter pools and was subject to microbial decay. The roots of the vegetation that died were delivered to the belowground litter pool. We tracked the amount of biomass that was killed by fire but not combusted so that we could calculate the indirect decomposition losses from fire, i.e., heterotrophic respiration from fire-induced mortality (Fig. 4). Losses to herbivores and fuel wood consumption are also included in the model. Herbivore consumption was calculated using a relation between consumption and foliar NPP

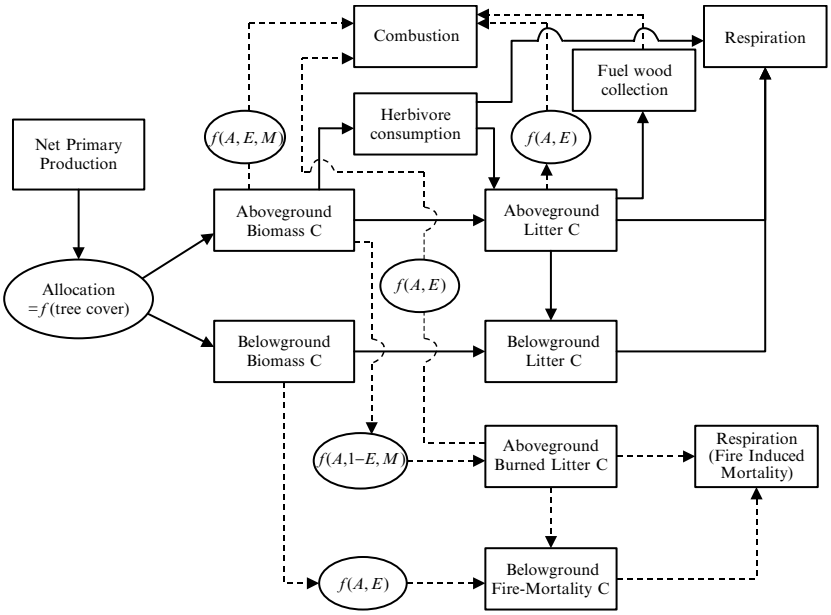

Fig. 4 Flowchart of fire processes in the CASA model. *A* is area burned, *E* is combustion factor, *M* is mortality. Dashed arrows represent fire-induced fluxes.

Table 1 Combustion and mortality factors for CASA model carbon pools

	Woody biomass			Herbaceous biomass		Litter	
Pool type	Leaves	Stems	Fine roots	Leaves	Fine roots	Coarse litter	Fine litter
Combustion factor*	0.90	0.20	0	0.90	0	0.40	0.95
Mortality factor	(% wood/(% wood + % herbaceous))^2			1	0.1	1	1

*Combustion factors based on data for Africa from Shea *et al*. (1996) and Hoffa *et al*. (1999).

(McNaughton *et al*., 1989; Randerson *et al*., 1996). Herbivore efficiency was assumed to be 50%, with the remaining C delivered to the fast decomposing litter pools. We accounted for the loss of fuel as a result of fuel wood consumption as follows: for any given country within the TRMM coverage area we multiplied the consumption of traditional fuel per capita (US Congress, 1992) by the population density in the grid cell (Center for International Earth Science Information Network, 2000) and subtracted this value from the coarse wood litter pool. The burning of fuel wood is not likely to be detected by the TRMM VIRS fire detection algorithm. We assumed no seasonality in fuel wood consumption and herbivore consumption. The model was spun up with the mean area burned for the four years, until the total yearly NPP equaled the sum of the potential losses and all carbon stocks were in equilibrium.

Tropical vegetation classification

For the purpose of exploring the dependence of fires on moisture regime and productivity across the tropics, we constructed a vegetation map based on mean annual precipitation (MAP) and satellite-derived tree cover (DeFries *et al*., 1999). We defined closed canopy broadleaf forest as areas where the amount of tree cover exceeded 70% and MAP exceeded 1500 mm, and open canopy moist woodlands as areas where the amount of tree cover was less than 70% (and again MAP exceeded 1500 mm). The other vegetation types were separated by different MAP values (Fig. 5; Table 2).

Results

Seasonality of fire activity and burned area estimates

The month of maximum fire activity was defined as the month with the maximum number of fire counts (and thus burned areas and typically emissions). Generally, the maximum occurred during the early to mid part of the dry season and had an equatorial asymmetry that was about 6 months out of phase with the Inter-Tropical Convergence Zone (ITCZ) (Fig. 6). For Africa, the TRMM VIRS fire counts showed the same latitudinal trend as

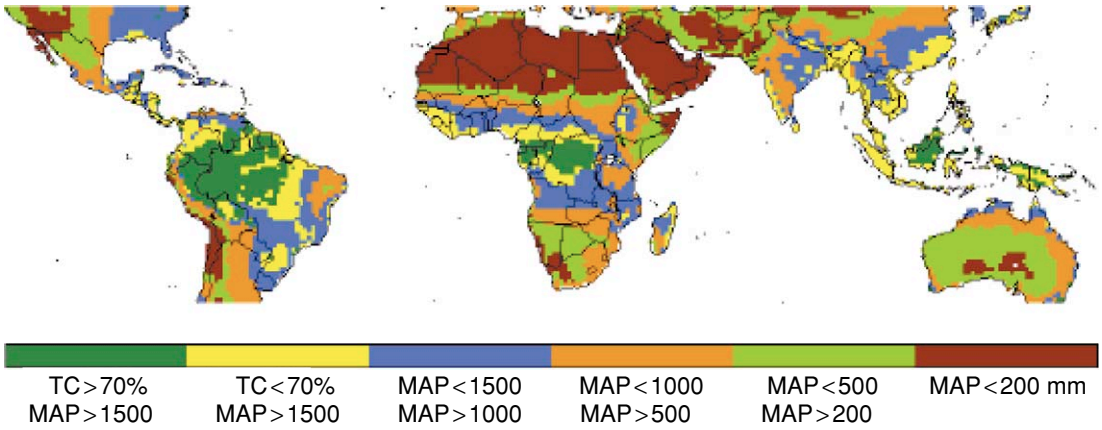

Fig. 5 A map of six tropical and subtropical classes was derived from tree cover (TC) and mean annual precipitation (MAP).

Table 2 Biome classification

Biome	MAP* range	% tree cover range†	average MAP (mm)	average % tree cover	Area (10^6 km^2)	Area (%)
1. Closed canopy broadleaf forest	>1500	73–84	2318	77	7.8	9
2. Open canopy moist woodland	>1500	14–64	2087	37	12.0	15
3. Intermediate woodland	1000–1500	8–54	1248	29	15.5	19
4. Wooded grassland	500–1000	1–41	743	17	15.3	19
5. Grassland/shrubland	200–500	0–12	333	3	15.2	18
6. Desert	<200	0–0	90	0	16.7	20

*Closed canopy broadleaf forest was defined as regions with MAP > 1500 and tree cover > 70%, whereas open canopy moist woodland had tree cover < 70%. All other vegetation classes were defined solely by the precipitation range defined in this column.
†Range given is the 10–90 percentile. The tree cover estimate was based on the AVHRR derived product from DeFries *et al*. (1999).

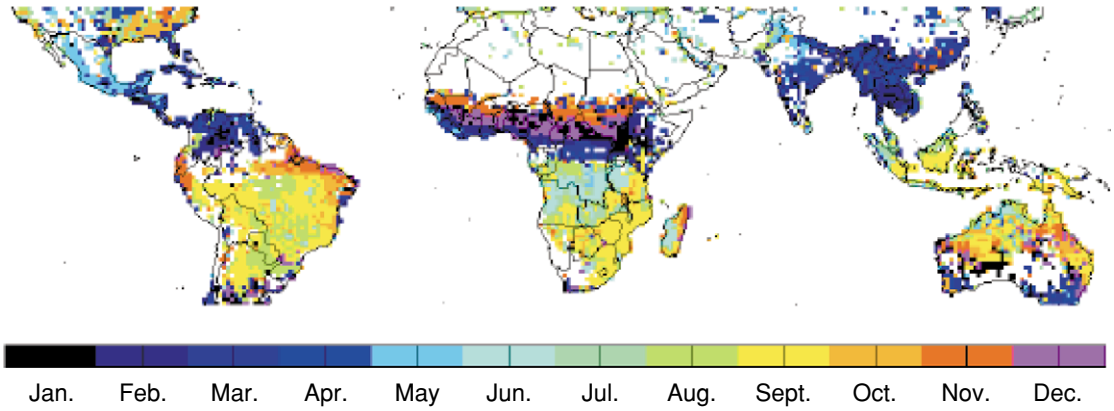

Fig. 6 Peak of fire season derived from the maximum of monthly TRMM fire counts.

found by Cahoon *et al*. (1992), although the maximum fire activity in the northern part of Africa occurred 1–2 months earlier, starting in November. In southern hemisphere Africa the month of maximum fire activity occurred in June on the west side of the continent, and in September on the east side of the continent. In the southern US, fire activity peaked in the fall (August–October) and in drier areas (i.e. Arizona, New Mexico, Texas) in spring (February–June). Spring was also the season with most fire activity in Central America. In Mexico the maximum fire activity occurred in the month of May for all 4 years (1998–2001). In northern

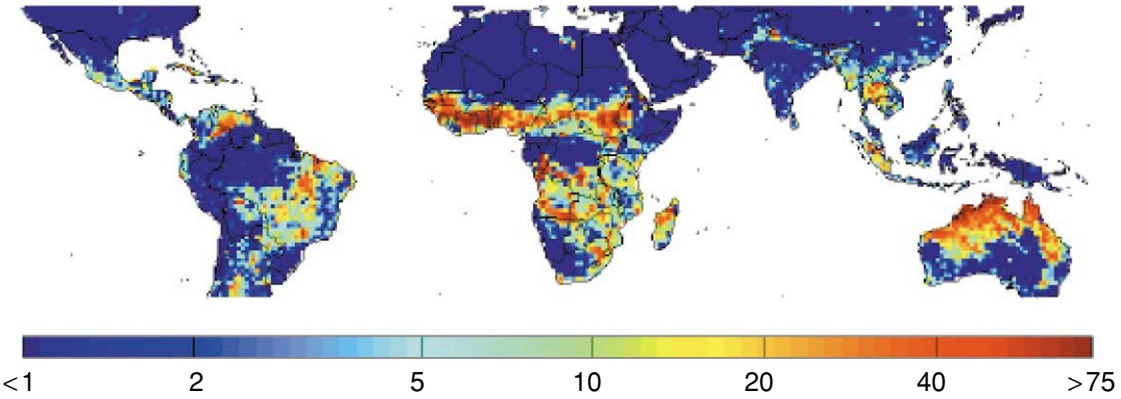

Fig. 7 Annual burned area (in percentage of each grid cell), averaged over the 1998–2001 period.

Table 3 A comparison of burned area and emission estimates for southern Africa from different sources

	Burned area (10^6 km^2 yr^{-1})	Emissions (Tg C yr^{-1})
Scholes *et al*. (1996) inventory (no specific time period)	3.99	252–785
Scholes *et al*. (1996) satellite (1989)*	1.68	80
Barbosa *et al*. (1999b) (1981–1983 and 1985–1991)†	1.54	205
GBA2000 (2000)‡	0.72	–
This study (1998–2001)§	1.16	516

*Forest clearing explicitly excluded.
†The mean of two scenarios presented by Barbosa *et al*. (1999b).
‡Global Burned Area 2000 project, Grégoire *et al*. (2002).
§Fuel wood consumption not included.

South America fire activity was greatest from January through March. In the central Amazon, fires peaked in August. To the north and east from the central Amazon, the month of maximum fire activity occurred at later times, with coastal areas showing the highest activity in October, in some years as late as December. Year to year variability in fire season was largest in Southeast Asia. In Eastern Borneo, for example, peak burning in 1998 occurred in February and March but in other years August and September were the months of highest fire activity. Generally, the mainland of Southeast Asia burned most frequently from January till March; Indonesia's burning season normally peaked during August and September. The situation in Australia was rather complex and also varied between years. Most burning occurred in northwest Australia from June to October, and in northeast Australia from October to December.

With the relationship between fire counts and burned area as described above, we calculated the fractional area of the grid cells that burned during the 1998–2001 period (Fig. 7). Our highest values were in the African countries of Ghana, Togo, and Benin where burned areas exceeded 75% in some grid cells each year. In terms of relative area, Australia burned most intensively with 15% of the continent burning each year as compared with Africa (9%) and South-America (5%). In terms of absolute area, the largest cumulative burned area occurred in Africa (2.81 million km^2 yr^{-1}). Table 3 summarizes burned area estimates for Southern Africa, including the estimate obtained here from TRMM and MODIS data.

Biomass and fuel estimates

Figure 8 shows the observed fuel accumulation after a fire event reported by Shea *et al*. (1996) for a savanna site in Kruger National Park, South Africa and the accumulation of fuel (here: all litter and herbaceous biomass) produced by our model for the co-located one degree grid cell. The post fire recovery trajectory and the absolute values of fuel load are similar, but may be biased if the FPAR and climate at the measured sites differed from the mean FPAR and climate used in the modelled $1^\circ \times 1^\circ$ grid cell.

Predicted aboveground carbon densities for the six biome types (ranging from closed canopy broadleaf forests to deserts) considered here are summarized in

Table 4. FPAR, NPP, biomass, and detritus all show increasing trends with increasing rainfall and moisture availability. Total aboveground carbon density is a measure of the total potential fuel load and includes woody and herbaceous biomass, leaf litter, and coarse woody debris. Values are divided into living woody and dead woody and into total herbaceous components. In herbaceous dominated biomes the woody biomass is often not included in reported estimates of fuel load because fire-induced mortality of the woody components is low (Crutzen & Andreae, 1990). Each biome type included a large range of carbon storage characteristics as indicated by the large standard deviations. The amount of biomass and litter combusted during a fire depends strongly on the combustion factor and mortality rate (Eqn (1)). In Table 4 these factors are given averaged for each biome. The average (biome level) combustion factor was calculated as the ratio between consumed carbon and carbon available for combustion (detritus and all biomass that actually died during the fire) and depended on the relative distribution of the different tissues with different combustion factors (Table 1). The aggregated combustion factor increased with aridity because there were fewer trees (with a relatively low combustion factor) in these regions, and because the fire-induced mortality of these trees was parameterized in our model to decrease with fractional tree cover (which is correlated with aridity).

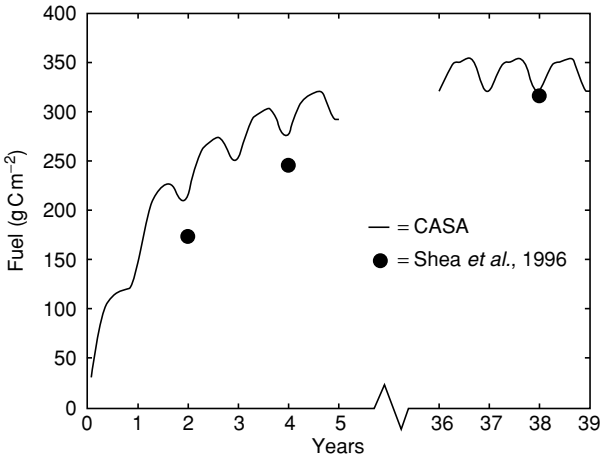

Fig. 8 Fuel load calculated by CASA compared with observations from three sites with savanna type vegetation cover burned 2, 4, and 38 years before measurements. Measurements were made in the Kruger National Park (lat. 25°15′13″S, lon. 31°14′00″E) as reported in Shea *et al*. (1996).

Table 4 Mean biome carbon fluxes, biomass and detritus densities, and model parameters for six different tropical and subtropical biomes

Biome	1	2	3	4	5	6	All
FPAR (–)	0.69	0.58	0.47	0.32	0.10	0.02	0.32
NPP (g C m^{-2} yr^{-1})	1194	971	757	467	123	19	496
Aboveground woody biomass (g C m^{-2})*†	9593 (2871)	3796 (2517)	2481 (1913)	1211 (1531)	133 (447)	13 (45)	2087
Aboveground woody detritus (g C m^{-2})*†	1641 (393)	615 (487)	416 (409)	222 (332)	40 (155)	6 (18)	358
Aboveground herbaceous biomass and detritus (g C m^{-2})*	134 (41)	240 (86)	227 (93)	198 (106)	107 (102)	38 (61)	152
Mortality of woody vegetation (%)‡	65	20	13	6	1	0	12
Combustion factor (–)‡	0.30	0.53	0.62	0.76	0.91	0.93	0.74
Fire return time (year)	89	10	8	11	24	332	16
Combustion flux (Tg C yr^{-1})	148	661	802	417	65	3	2096
Combustion flux (g C m^{-2} yr^{-1})	19.1	54.4	50.0	26.6	4.2	0.2	24.3
Indirect loss flux (g C m^{-2} yr^{-1})§	37.1	35.0	23.9	7.8	0.5	0.2	14.1
Microbial respiration (% of NPP)	90.3	84.0	84.0	87.4	93.5	98.0	86.5
Combustion (% of NPP)	1.6	5.6	6.6	5.7	3.4	0.9	4.9
Indirect loss (% of NPP)§	3.1	3.6	3.1	1.7	0.3	0.1	2.8
Herbivory (% of NPP)	4.7	5.3	4.8	4.2	2.3	0.8	4.7
Fuel wood consumption (% of NPP)	0.2	1.5	1.4	1.1	0.5	0.2	1.1

*The standard deviation is given in parentheses.

†Aboveground woody biomass includes all living tissues (stems and leaves), woody detritus includes coarse woody debris and fine litter derived from the woody fraction of the vegetation. Mortality and combustion factors are aggregated values over all relevant carbon pools within each grid cell and over all grid cells within each biome (Eqn (1), Table 1).

§The indirect loss is a microbial respiration flux from vegetation killed but not combusted by fire.

Table 5 Regional variability in burned area, carbon fluxes and fire emissions

Region	N-America*	S-America*	N-Africa*	S-Africa*	SE-Asia†	Australia
Area (10^6 km^2)	9.2	13.6	20.1	9.8	8.5	8.0
FRT‡ (years)	30	18	12	9	22	7
Burned area (10^6 km^2 yr^{-1})	0.30	0.74	1.67	1.15	0.39	1.18
Total NPP (Pg C yr^{-1})	6.6	12.2	5.9	6.5	6.6	1.6
GSNF (Pg C yr^{-1})	0.84	1.51	1.05	1.12	0.77	0.34
Combustion flux (Pg C yr^{-1})	0.18	0.50	0.51	0.52	0.22	0.15
Closed canopy broadleaf forest share (%)§	3	19	2	1	11	0

*North defined as north of the equator, south as south of the equator.
†Southeast Asia defined as Asia east of Pakistan and south of China.
‡Fire return time (FRT) was obtained from the average of satellite observations during the TRMM era (1998–2001).
§Contribution of closed canopy broadleaf forest emissions to total emissions.

Direct and indirect carbon losses

Over the 1998–2001 period, CASA estimates of global NPP were 56 Pg C yr^{-1}, of which 42 Pg C yr^{-1} or 75% occurred within the coverage area of the TRMM satellite (38°N–38°S). The relative amounts of carbon lost through the various pathways are shown in Table 4. In areas with a low fire frequency and low population density such as the closed canopy broadleaf forests (biome 1) and deserts (biome 6) most of the carbon fixed through NPP returned to the atmosphere via microbial respiration whereas in the more densely populated and herbaceous biomes (biomes 2, 3, and 4) the role of fire and fuel wood collection played a more important role. The highest fractions of NPP lost to fire were almost 25% in annually burning savannas (i.e. those regions in Fig. 7 with very high burned area). Heterotrophic respiration from fire-induced mortality was generally lower than direct combustion, although in densely forested areas it was higher and in some cases exceeded direct combustion by a factor of four (Table 4). Herbivory was dependent on the amount of NPP allocated to foliage so it was highest in places with high NPP but low tree cover such as the equatorial grasslands where in some cases up to 28% of NPP was lost to herbivores.

Total carbon loss from fires was calculated at 2.1 Pg C yr^{-1} with an extra 0.5 Pg C yr^{-1} from fuel wood consumption. Our estimates also included the burning of agricultural waste since in this analysis we did not differentiate between agriculture and non-agricultural lands. On a continental scale, most emissions originated in Africa (45% with fuel wood consumption, 49% without), and were almost evenly distributed within Africa north and south of the equator. Table 5 summarizes the distribution of emissions over different continents. During the 4-year study period 0.15 Pg C yr^{-1} was lost from closed canopy broadleaf forest (tropical forest) fires, and fires in forested areas were most important in South America and Southeast Asia.

Seasonality of net biome production

The relative importance of NPP, heterotrophic respiration, and fires on seasonal net biome production (NBP) are shown in Fig. 9 for six regions. The opposite phase between the hemispheres is obvious for the Americas and Africa. In tropical and subtropical regions, precipitation is often the limiting factor for both NPP and heterotrophic respiration. With the onset of the dry season, NPP and heterotrophic respiration decrease and the fire activity increases. When fires were excluded from the biogeochemical model, the seasonality in NBP was still obvious but the amplitude was dampened (Fig. 10). This behavior was not observed for the whole of Southeast Asia and Australia since the season with highest productivity did not occur at the same time over the entire region. But for smaller areas within these two regions with similar seasonality the same patterns were observed (not shown) as in the Americas and Africa. CASA simulations revealed that fires increased the seasonal amplitude of NBP in tropical regions because fires occurred when precipitation was low and heterotrophic respiration from soils exceeded carbon gain from NPP. Currently little observational data exist for evaluating the relative response of heterotrophic respiration and NPP to soil moisture variability on seasonal and interannual timescales in savanna and tropical forest ecosystems (Randerson *et al.*, 2002).

The growing season net flux (GSNF, defined as the net atmosphere–biosphere flux integrated over the growing season, i.e., during months with a negative net flux to the atmosphere) was calculated for model runs with and without fires (Table 6). GSNF was highest in savannas with a MAP of 1000–1500 mm. Excluding fires lowered

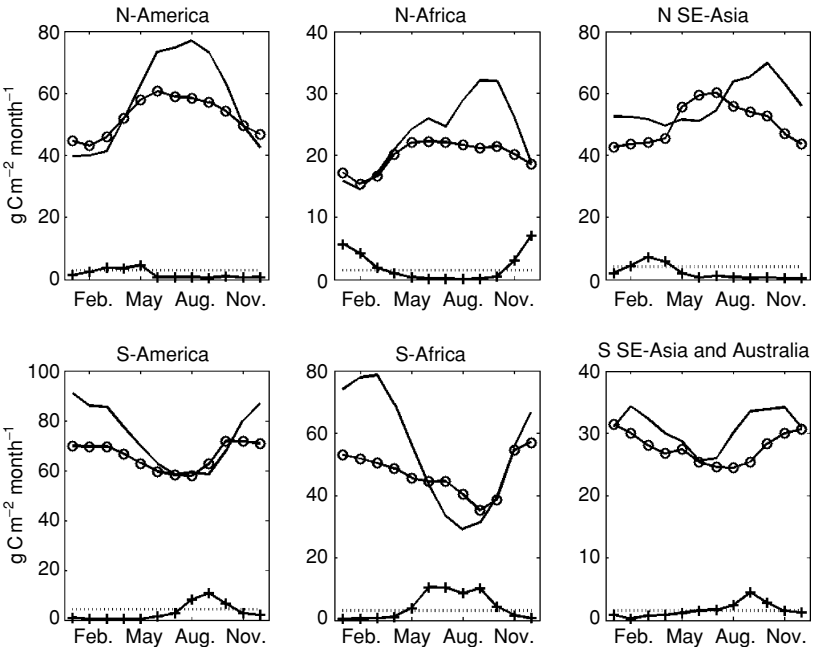

Fig. 9 Seasonal carbon fluxes for different regions. The solid line represents NPP, the circled line microbial respiration, plusses direct fire emissions, and the dashed line the sum of herbivore heterotrophic respiration and fuel wood consumption. Northern regions are defined as all areas north of the equator.

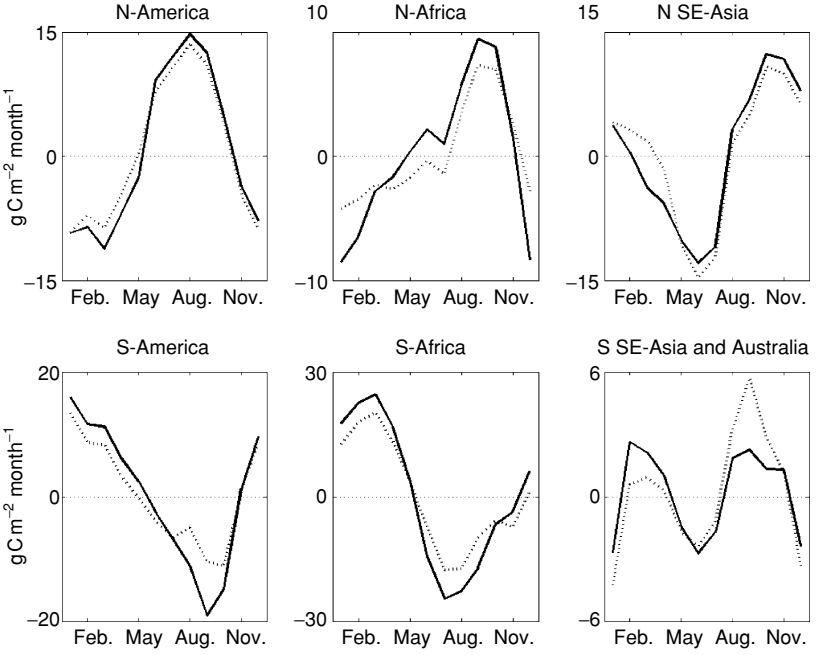

Fig. 10 Seasonal net biome production for model runs with (solid line) and without (dashed line) fire influences. Positive values represent a flux towards the biosphere, negative towards the atmosphere.

GSNF, on average, by 12%, and by over 15% in moist and intermediate woodland ecosystems.

Sensitivity to burned area algorithm

Carbon emission rates are highly sensitive to assumptions about burned area in closed canopy forests. For example, if the burned area per fire count relationship was increased in regions with tree cover greater than 35% (scenario 1, Table 7) emissions increased by 50%, even though the global burned area increased by only 27%. When scaling our burned area for southern Africa to the values reported in two other studies (Scholes *et al*., 1996; Barbosa *et al*., 1999b) and extrapolating that relationship to the TRMM domain we found an increase in emissions of 38% with an increase of area burned of 55% (scenario 2).

Not surprisingly, fire frequency and biomass and litter densities are inversely related. Table 7 shows the

Table 6 Growing season net flux (GSNF, in $g\,C\,m^{-2}\,yr^{-1}$) for different biomes

Biome	GSNF without fire*	GSNF with fire	% increase
1. Closed canopy broadleaf forest	73	79	8
2. Open canopy moist woodland	104	123	16
3. Intermediate woodland	120	141	15
4. Wooded grassland	89	98	9
5. Grassland/shrubland	31	32	3
6. Desert	6	6	0
All	67	77	12

*Fuel wood consumption also excluded.

Table 7 Sensitivity of carbon density and emissions to changes in fire frequency

		Scenario*		
		Primary model run	1	2
Africa	Burned area (million $km^2\,yr^{-1}$)	2.81	3.50	4.30
	Woody biomass†	1831	1353	1492
	Woody litter†	313	251	269
	Herbaceous biomass and litter†	189	175	170
	Woody combustion ($Tg\,C\,yr^{-1}$)‡	420	668	559
	Herbaceous combustion ($Tg\,C\,yr^{-1}$)	606	751	820
	Total combustion ($Tg\,C\,yr^{-1}$)‡	1026	1419	1379
38°N–38°S	Burned area (million $km^2\,yr^{-1}$)	5.50	6.99	8.50
	Woody biomass†	2374	1962	2151
	Woody litter†	399	351	375
	Herbaceous biomass and litter†	220	210	207
	Woody combustion ($Tg\,C\,yr^{-1}$)‡	968	1673	1323
	Herbaceous combustion ($Tg\,C\,yr^{-1}$)	1128	1448	1563
	Total combustion ($Tg\,C\,yr^{-1}$)‡	2096	3121	2886

*Different scenarios from Fig. 3.
†Biomass and litter for savanna type biomes (2, 3, and 4 from Table 2), values include only aboveground carbon, in $g\,C\,m^{-2}$.
‡Fuel wood consumption not included.

aboveground carbon density of the different fuel loads for the different burned area (and thus fire frequency) scenarios. When comparing our primary model run and scenario 2 the area burned increased by over 50%, but carbon density in the savanna type biome decreased by only 10%. For the herbaceous component, in which regrowth reaches steady state more quickly, the decrease was even smaller, about 5%. The relative change in carbon density in Africa was larger than the change in the global tropics and subtropics. This is because fires are more prevalent in Africa and much of the vegetation is still recovering from a previous fire.

The sensitivity of fuel properties and thus emissions to a change in fire frequency depends on the recovery trajectory of the fuel and at what point on this trajectory the next fire occurs. Normally, the biomass trajectory has an asymptotical shape (Fig. 8) whose slope depends on NPP and on allocation, herbivory, and rates of decomposition. The longer the fire return time is as compared to the timescale for biomass accumulation, the less sensitive the fuel density will be but the more sensitive the emissions will be to a change in fire frequency. For example, in an ecosystem that reaches biomass steady state after a period of several decades in the absence of fire (similar to the one presented in Fig. 8) a change in fire return time from 50 to 25 years would almost double the emissions (when integrated over a period of centuries) but would have a very small effect on the average fuel properties. On the other hand, halving the fire return time from 2 years to 1 year in this same ecosystem would have a small effect on emissions but a large effect on average biomass and litter densities.

Discussion

Burned area estimation

Fires burned the largest areas in the biomes 2, 3, and 4 defined in Table 2. In these biomes NPP was moderate to high, the overstorey canopies were open (allowing the fuel to dry out), and there was a distinct dry season. Another important factor may have been that in many of these areas the population density is relatively high, and humans use fire as a tool to control the vegetation cover. Similar to Scholes *et al*. (1996), who compared an inventory method with a remote sensing approach for southern Africa, we found that our satellite derived burned areas were lower than those derived from previously reported inventory-based approaches. Our burned area value for southern Africa was ~31% lower than reported by Scholes *et al*. (1996) and slightly smaller than the lower scenario presented by Barbosa *et al*. (1999b). The two scenarios described by Barbosa *et al*. (1999b) estimated burned area for all of Africa to be between 3.0×10^6 and $5.5 \times 10^6\,km^2$. Our estimate for the same region was $2.8 \times 10^6\,km^2$. A global burned area data set (GBA2000) for the year 2000 has recently been released which is based on fire information derived from the VEGETATION instrument on board the SPOT 4 satellite (Grégoire *et al*., 2002). The GBA2000 burned area for southern Africa is less than half of the values given by Scholes *et al*. (1996) and Barbosa *et al*. (1999b) and nearly 40% lower than our estimate (Table 3). When comparing these different studies it is important to recognize that interannual variability in area burned may be considerable (Barbosa *et al*., 1999b) so the differences may be in part a result of the different time periods of the satellite observations.

The fire return times (equivalent to the reciprocal of the average fraction of a grid cell burned in a year when averaged over long periods) are given in Table 4 for the different biome classes and in Table 5 for different regions. One problem when comparing these results with observed fire return times at specific sites is that the latter are applicable to relatively homogeneous vegetation cover while the satellite measured fire return times may include a mixture of cover types within a grid cell. For example, if 50% of a grid cell consists of annually burning savanna and the remainder is urban or bare soil where no fires occur (FRT is infinite) then the estimated fire return time as measured by a satellite for the grid cell would be 2 years instead of one. In addition, given the large interannual variability in tropical emissions in many regions (Barbosa *et al*., 1999b), our results are likely to be biased by the relatively short sampling interval of our analysis. The fire return time of 90 years for closed canopy broadleaf forests that we obtained here is likely to be biased because we sampled the tail of the 1997–1998 ENSO season during which fires burned into tropical forests. Alternatively, ongoing deforestation may be radically changing the FRT in many closed tropical forests (Cochrane *et al*., 1999; Nepstad *et al*., 1999).

Biomass and fuel loads

Ecological inventory studies of savannas often report biomass as all living tissues (e.g. Olson *et al*., 1983) whereas studies in the fire context often report biomass in a savanna as all above ground organic matter that can be combusted (e.g. Scholes *et al*., 1996). The latter will include litter but not the trees since they are often not killed by fire. This difference in terminology makes it difficult to directly compare field studies across disciplines. Here we defined the potential fuel content or fuel load (organic matter available for combustion) as all above ground herbaceous biomass, above ground woody biomass scaled by the fire mortality factor, coarse woody debris, and litter (Eqn (1)). In herbaceous biomes with lower density tree cover the woody biomass is assigned a low fire mortality value (Eqn (1), Tables 1 and 4) and thus contributes relatively little to the fuel load while in the more wooded biomes the fire mortality rate is higher so the fuel load is higher. In general, our fuel amounts for savannas and grasslands are higher than the mean values reported by others for Africa (Scholes *et al*., 1996; Barbosa *et al*., 1999b). Our values are averages over whole biomes and show large ranges (note the high standard deviation in Table 4); the more frequently burning grid cells exhibit fuel loads closer or even lower than reported in these other studies. Furthermore, our model uses the mean FPAR observed over the whole $1^\circ \times 1^\circ$ grid cell to calculate biomass and fuel loads. Variability of FPAR, NPP and associated fuel loads within a grid cell may bias our results. For example, small areas of dense vegetation cover such as might occur along water courses in an otherwise sparsely vegetated region could boost grid cell average FPAR, NPP and thus estimated fuel loads. The trajectory of fuel amount accumulation after a savanna fire predicted by our model is similar to that observed in one study from southern Africa (Fig. 8). Our averaged biomass levels for savanna (biomes 2–4, 1700–5350 $g\,C\,m^{-2}$) and closed canopy broadleaf forests (13 000 $g\,C\,m^{-2}$) are comparable to measured values (tropical savanna vegetation types (ecosystem codes 41, 43, 59, and 32): 1000–6000 $g\,C\,m^{-2}$; tropical closed canopy broadleaf forest (ecosystem codes 29, 33, and 73): 12 000 $g\,C\,m^{-2}$ (Olson *et al*., 1983).

Annual emissions

Our emission estimates for southern Africa are higher than those reported by Scholes *et al*. (1996) and Barbosa

et al. (1999b) even though our burned area estimates are smaller (Table 3). The main reasons are that in our model, woody vegetation contributed substantially to emissions in savanna grid cells, and that the average biomass and detritus properties predicted by CASA were higher than the values used in these previous studies. The much lower burned areas given in the GBA2000 data set would have reduced our emissions estimates by about 32%.

When we applied a higher burned area per fire count value in wooded areas (scenario 1), our emission estimate for the Legal Amazon increased from $0.23\,Pg\,yr^{-1}$ to $0.54\,Pg\,yr^{-1}$. This is still $0.17\,Pg\,yr^{-1}$ lower than the value found by Potter *et al*. (2001) for the 1992–1993 period, mainly because our model had lower combustion factors. The relatively small contribution of closed canopy broadleaf forest to total tropical emissions may be partly attributed to our biome classification in which the forests were less extensive than in other classification approaches (Fig. 5).

Seasonal dynamics

The seasonality of NPP and heterotrophic respiration fluxes were somewhat parallel because soil moisture and temperatures favorable to plant growth and productivity also stimulated microbial activity. The relatively small month-to-month changes in temperature had a relatively minor effect on NPP in our model. Rather, most of the seasonality in NPP resulted from soil moisture stress effects on prescribed FPAR and derived ε. Similarly, seasonality in heterotrophic respiration in the tropics and subtropics was largely driven by soil moisture stress on decomposition. The net result was that NPP and respiration showed parallel seasonal changes though the amplitude was larger for NPP. The higher seasonal amplitude in NPP in our model results in positive NBP (net uptake of carbon from the atmosphere) during the growing season and negative NBP (net release to the atmosphere) during the dry season. Introducing the effects of fire causes the seasonal amplitude in NBP to increase because fires, which tend to occur mostly during the dry season, contribute to greater net release of carbon. During the growing season respiration was reduced because detrital carbon pools were smaller, having been consumed by fire in the previous dry season, and leading to greater net uptake of carbon.

Uncertainties

The variables necessary to calculate carbon losses from fire (burned area, fuel loading, combustion factors, and fire-induced mortality rates) are all highly uncertain and more testing against ground truth data will be necessary to establish confidence in our ability to accurately estimate emissions from fires at regional to global scales. Of these uncertainties, burned area is probably the most significant for emission estimation. Judging from the range of values for southern Africa (Table 3) uncertainties in area burned estimates may be as high as 50% or more.

Our model produces higher average fuel loads than used in other studies for southern Africa which results in higher predicted emissions despite our lower estimates of burned area. It is difficult to assess the uncertainties in fuel loads because site observations are not directly comparable to our regional estimates. Quantifying biomass and detritus is not only an important requirement for estimating fuel loads but also is necessary in order to identify terrestrial sources and sinks for atmospheric CO_2 (e.g. Pacala *et al*., 2001). Further work on this topic is therefore a high science priority.

The combustion factors used for leaves and litter probably do not contribute much to the uncertainty since they are almost always observed to be close to unity, and field studies have provided direct measurement (i.e. Shea *et al*., 1996; Guild *et al*., 1998; Hoffa *et al*., 1999; Carvalho *et al*., 2001). In contrast, the combustion factors for wood and wood litter are not well known. The small number of reported values varies between 0 and 1 but is generally between 0 and 0.5. Mortality rates for mature trees are known to be very low in savanna areas (Trollope *et al*., 1990) and higher in wooded areas but the actual rates are not well known. Our method of modelling the mortality should be viewed as a simple approach for capturing the dependence of tree mortality on tree cover. By highlighting its importance with respect to fire emissions estimates we hope to encourage further work to quantify fire induced mortality.

Variability in burn severity within an area burned produces uncertainty in our study that can be ascribed to either the area burned estimation or the combustion and mortality factors. When more information is available that would allow estimation of the patchiness within fire scars it would be preferable to include this in the form of an additional multiplicative factor in Eqn (1).

When all of these uncertainties in the calculation of emissions are taken into account, an uncertainty range of greater than 50% is likely for estimates of mean annual carbon emissions from tropical ecosystems, even though TRMM represents a new and powerful constraint on regional and interannual variability. Ultimately, top down approaches that consider atmospheric concentrations of CO_2 together with other tracers like CO may allow us to constrain emissions estimates on regional and continental scales (Bergamaschi *et al*., 2000; Langenfelds *et al*., 2002).

Conclusions

The TRMM VIRS satellite record provides new constraints on temporal and spatial variability in carbon emissions from fire in the global tropics. We estimated that for the region observed by the TRMM satellite (38°N to 38°S), 2.6 Pg C yr^{-1} (or 6% of NPP) was lost as direct emissions (vegetation fires and fuelwood combustion) and an extra 1.2 Pg C yr^{-1} (or 3% of NPP) was lost as respiration from fire-induced mortality. These results, as with all other studies of this type, are highly uncertain especially because of uncertainties in estimates of burned areas and fuel loads.

Fires were significant in all biomes, but the woody savanna type biome with 1000–1500 mm MAP (biome 3) showed the shortest FRT (8 years), slightly shorter than biomes with higher MAP (biome 2; 10 years) or lower MAP (biome 4; 11 years). A further increase or decrease in MAP resulted in a longer FRT because the environment was either too moist (associated with a reduction in the length of the fire season and an increase in tree cover density) in the former case or low fuel loads limiting the frequency of fires in the latter. The indirect to direct loss ratio was highest in the wettest biomes, where amount and mortality of woody biomass with a relatively low combustion factor was high, leaving much uncombusted fuel after a fire to respire. The indirect to direct loss ratio decreased with decreasing MAP.

Our approach, which used additional satellite and climate data to derive estimates of NPP and carbon stocks, appeared to capture much of the spatial variability in fuel loads and emissions that occurs in tropical savannas, woodlands, and closed forests. Our results reveal how fires can have a significant effect on seasonal dynamics by magnifying the amplitude of the net biome production altering the corresponding atmospheric CO_2 signal. As a next step, we plan to use TRMM and MODIS satellite data to explore interannual variability in emissions, and in particular, shifts in fire frequency and emissions associated with El Nino.

Acknowledgements

This work was funded in part by NASA EOS-IDS grants NRA99-OES-04 (PI: P. Kasibhatla) and NAG5-9462 (PI: J.T. Randerson).

References

Barbosa PM, Gregoire JM, Pereira JMC (1999a) An algorithm for extracting burned areas from time series of AVHRR GAC data applied at a continental scale. *Remote Sensing of Environment*, **69**, 253–263.

Barbosa PM, Stroppiana D, Gregoire JM *et al.* (1999b) An assessment of vegetation fire in Africa (1981–1991): burned areas, burned biomass, and atmospheric emissions. *Global Biogeochemical Cycles*, **13**, 933–950.

Behrenfeld MJ, Randerson JT, McClain CR *et al.* (2001) Biospheric primary production during an ENSO transition. *Science*, **291**, 2594–2597.

Bergamaschi P, Hein R, Heimann M *et al.* (2000) Inverse modeling of the global CO cycle 1. Inversion of CO mixing ratios. *Journal of Geophysical Research–Atmospheres*, **105**, 1909–1927.

Bishop JKB, Rossow WB (1991) Spatial and temporal variability of global surface solar irradiance. *Journal of Geophysical Research–Oceans*, **96**, 16839–16858.

Cahoon DR, Stocks BJ, Levine JS *et al.* (1992) Seasonal distribution of African savanna fires. *Nature*, **359**, 812–815.

Carvalho JA, Costa FS, Gurgel Veras CA *et al.* (2001) Biomass fire consumption and carbon release rates of rainforest-clearing experiments conducted in northern Mato Grosso, Brazil. *Journal of Geophysical Research–Atmospheres*, **106**, 17877–17887.

Center for International Earth Science Information Network (CIESIN) Columbia University, International Food Policy Research Institute (IFPRI); and World Resources Institute (WRI) (2000) Gridded Population of the World (GPW), Version 2. Palisades, NY: CIESIN, Columbia University. Available at. http://sedac.ciesin.columbia.edu/plue/gpw.

Cochrane MA, Alencar A, Schulze MD *et al.* (1999) Positive feedbacks in the fire dynamic of closed canopy tropical forests. *Science*, **284**, 1832–1835.

Crutzen PJ, Andreae MO (1990) Biomass burning in the tropics – Impact on atmospheric chemistry and biogeochemical cycles. *Science*, **250**, 1669–1678.

Defries RS, Hansen MC, Townshend JRG *et al.* (2000) A new global 1-km dataset of percentage tree cover derived from remote sensing. *Global Change Biology*, **6**, 247–254.

DeFries RS, Townshend JRG, Hansen MC (1999) Continuous fields of vegetation characteristics at the global scale at 1-km resolution. *Journal of Geophysical Research–Atmospheres*, **104**, 16911–16923.

Delmas RA, Druilhet A, Cros B *et al.* (1999) Experiment for regional sources and sinks of oxidants (EXPRESSO): An overview. *Journal of Geophysical Research–Atmospheres*, **104**, 30609–30624.

Eva H, Lambin EF (1998) Remote sensing of biomass burning in tropical regions: sampling issues and multisensor approach. *Remote Sensing of Environment*, **64**, 292–315.

Field CB, Behrenfeld MJ, Randerson JT *et al.* (1998) Primary production of the biosphere: Integrating terrestrial and oceanic components. *Science*, **281**, 237–240.

Field CB, Randerson JT, Malmstrom CM (1995) Global net primary production – Combining ecology and remote-sensing. *Remote Sensing of Environment*, **51**, 74–88.

Giglio L, Kendall JD, Mack R (in press) A multi-year active fire data set for the tropics derived from the TRMM VIRS. *International Journal of Remote Sensing*.

Giglio L, Kendall JD, Tucker CJ (2000) Remote sensing of fires with the TRMM VIRS. *International Journal of Remote Sensing*, **21**, 203–207.

Gill AM (1981) Fire adaptive traits of vascular plants. In: *Fire Regimes and Ecosystem Properties* (eds Mooney HA, Bonnickson JM, Christensen NL *et al.*), pp. 208–230. US Department of Agriculture and Forest Science, General Technical Report, Washington, DC.

Grégoire J-M, Tansey K, Silva JMN (in press) The GBA2000 initiative: developing a global burned area database from SPOT-VEGETATION imagery. *International Journal of Remote Sensing*.

Guild LS, Kauffman JB, Ellingson LJ *et al.* (1998) Dynamics associated with total aboveground biomass, C, nutrient pools, and biomass burning of primary forest and pasture in Rondonia, Brazil during SCAR-B. *Journal of Geophysical Research–Atmospheres*, **103**, 32091–32100.

Hao WM, Liu MH (1994) Spatial and Temporal Distribution of Tropical Biomass Burning. *Global Biogeochemical Cycles*, **8**, 495–503.

Hao WM, Liu MH, Crutzen PJ (1990) Estimates of annual and regional releases of CO_2 and other trace gases to the atmosphere from fires in the tropics, based on the FAO statistics for the period 1975–1980. In: *Fire in the Tropical Biota: Ecosystem Processes and Global Challenges, Ecol. Studies 84* (ed. Goldammer JG), pp. 440–462. Springer-Verlag, New York.

Hoffa EA, Ward DE, Hao WM *et al.* (1999) Seasonality of carbon emissions from biomass burning in a Zambian savanna. *Journal of Geophysical Research–Atmospheres*, **104**, 13841–13853.

Kasischke ES, Christensen NL, Stocks BJ (1995) Fire, global warming, and the carbon balance of boreal forests. *Ecological Applications*, **5**, 437–451.

Kummerow C, Barnes W, Kozu T *et al.* (1998) The tropical rainfall measuring mission (TRMM) sensor package. *Journal of Atmospheric and Oceanic Technology*, **15**, 809–817.

Langenfelds RL, Francey RJ, Pak BC *et al.* (2002) Interannual growth rate variations of atmospheric CO_2 and its $d^{13}C$, H_2, CH_4, and CO between 1992 and 1999 linked to biomass burning. *Global Biogeochemical Cycles*, **16** (3), 1048, doi: 10.1029/2001GV001466.

Leemans R, Cramer WP (1990) The IIASA database for mean monthly values of temperature, precipitation and cloudiness of a global terrestrial grid. *International Institute of Applied System. Anal Laxenburg, Austria*, 60, pp.

Lindesay JA, Andreae MO, Goldammer JG *et al.* (1992) International Geosphere–Biosphere Programme/International Global Atmospheric Chemistry SAFARI-92 field experiment: Background and overview. *Journal of Geophysical Research–Atmospheres*, **101**, 23521–23530.

McNaughton SJ, Oesterheld M, Frank DA *et al.* (1989) Ecosystem-level patterns of primary productivity and herbivory in terrestrial habitats. *Nature*, **341**, 142–144.

Medina E, Silva FS (1990) Savannas of northern South America: a steady state regulated by water–fire interactions on a background of low nutrient availability. *Journal of Biogeography*, **17**, 403–413.

Menaut JC, Abbadie L, Lavenu F *et al.* (1991) *Global Biomass Burning: Atmospheric, Climatic, and Biospheric Implications* (ed. Levine JS). MIT press, Cambridge, MA.

Nepstad DC, Verissimo A, Alencar A *et al.* (1999) Large-scale impoverishment of Amazonian forests by logging and fire. *Nature*, **398**, 505–508.

Olson JS, Watts JA, Allison LJ (1983) *Carbon in Live Vegetation of Major World Ecosystems*. Report ORNL-5862. Oak Ridge National Laboratory, Oak Ridge.

Pacala SW, Hurtt GC, Baker D *et al.* (2001) Consistent land- and atmosphere-based US carbon sink estimates. *Science*, **292**, 2316–2320.

Parton WJ, Scurlock JMO, Ojima DS *et al.* (1993) Observations and modeling of biomass and soil organic-matter dynamics for the grassland biome worldwide. *Global Biogeochemical Cycles*, **7**, 785–809.

Pereira JMC, Pereira BS, Barbosa P *et al.* (1999) Satellite monitoring of fire in the EXPRESSO study area during the 1996 dry season experiment: active fires, burnt area, and atmospheric emissions. *Journal of Geophysical Research–Atmospheres*, **104**, 30701–30712.

Potter C, Genovese VB, Klooster S *et al.* (2001) Biomass burning losses of carbon estimated from ecosystem modeling and satellite data analysis for the Brazilian Amazon region. *Atmospheric Environment*, **35**, 1773–1781.

Potter CS, Randerson JT, Field CB *et al.* (1993) Terrestrial ecosystem production – A process model based on global satellite and surface data. *Global Biogeochemical Cycles*, **7**, 811–841.

Randerson JT, Collatz GJ, Fessenden JE *et al.* (2002) A possible global covariance between terrestrial gross primary production and ^{13}C discrimination: consequences for the atmospheric ^{13}C budget and its response to ENSO. *Global Biogeochemical Cycles*, **16**, 1136.

Randerson JT, Still CJ, Ballé JJ *et al.* (2002) Carbon isotope discrimination of arctic and boreal biomes inferred from remote atmospheric measurements and a biosphere–atmosphere model. *Global Biogeochemical Cycles*, **16** (3), 1028, doi: 10.1029/2001GB001435.

Randerson JT, Thompson MV, Malmstrom CM *et al.* (1996) Substrate limitations for heterotrophs: implications for models that estimate the seasonal cycle of atmospheric CO_2. *Global Biogeochemical Cycles*, **10**, 585–602.

Scholes RJ, Kendall J, Justice CO (1996) The quantity of biomass burned in southern Africa. *Journal of Geophysical Research–Atmospheres*, **101**, 23667–23676.

Seiler W, Crutzen PJ (1980) Estimates of gross and net fluxes of carbon between the biosphere and the atmosphere from biomass burning. *Climatic Change*, **2**, 207–247.

Setzer AW, Pereira MC (1991) Amazonia biomass burning in 1987 and an estimate of their tropospheric emissions. *Ambio*, **20**, 19–22.

Shea RW, Shea BW, Kauffman JB *et al.* (1996) Fuel biomass and combustion factors associated with fires in savanna ecosystems of South Africa and Zambia. *Journal of Geophysical Research–Atmospheres*, **101**, 23551–23568.

Siegert F, Ruecker G, Hinrichs A *et al.* (2001) Increased damage from fires in logged forests during droughts caused by El Nino. *Nature*, **414**, 437–440.

Trollope WSW, Potgieter ALF, Zambatis N (1990) *Characterization of Fire Behavior in the Kruger Nation Park*. Final report of National Parks Board, Kruger National Park, South Africa.

US Congress Office of Technology Assessment (1992) *Fueling Development: Energy Technologies for Developing Countries, OTA-E-516*. US Government Printing Office, Washington, DC.